INTERNATIONAL JOURNAL OF CLIMATOLOGY
Int. J. Climatol. **30**: 1526–1537 (2010)
Published online 18 August 2009 in Wiley InterScience
(www.interscience.wiley.com) DOI: 10.1002/joc.1999

Spatial–temporal dynamics of precipitation extremes in southern Portugal: a geostatistical assessment study

R. M. Durão,[a]* M. J. Pereira,[a] A. C. Costa,[b] J. Delgado,[c] G. del Barrio[d] and A. Soares,[a]

[a] *Instituto Superior Técnico, CERENA, Av. Rovisco Pais, 1049-001 Lisboa, Portugal*
[b] *Universidade Nova de Lisboa, ISEGI; Campus de Campolide, 1070-312 Lisboa, Portugal*
[c] *Dpto. Ingeniería Cartográfica, Geodésica y Fotogrametría, Universidade de Jaén, Spain*
[d] *CSIC-Consejo Superior de Investigaciones Científicas, EEZA – Estación Experimental de Zonas Aridas; General Segura, 1 – 04001 Almería, Spain*

ABSTRACT: Most of the recent studies and projections of precipitation patterns, based on records observed in the past and climate change scenarios for the Mediterranean basin, suggest a relatively slow decrease in rainfall amounts over the years but an increase in the frequency of extreme precipitation events. These are key factors in desertification processes and these will cause social and environmental impacts in the short term, mainly because changes in heavy rainfall events may have severe implications and impacts on soil erosion, resulting in increased risk of soil degradation.

The main objective of the present work is to evaluate the spatial–temporal dynamics of extreme precipitation events in southern Portugal, using a direct sequential simulation algorithm (DSS models) in order to assess the relationships between spatial and temporal extreme rainfall patterns. Local probability density functions (pdfs) and spatial uncertainty are evaluated by a set of equiprobable simulated images of the chosen extreme precipitation indices.

The used dataset in this work comprises a set of 105 station records of observed daily precipitation within the period 1961–2000. Two indices of extreme precipitation were selected: one representing the frequency of extremely heavy precipitation events (R30) and another characterizing the occurrence of dry events (RL10), both obtained from observed daily precipitation series.

Results show that the spatial continuity of extreme precipitation events has increased in the last 40 years in southern Portugal. It also demonstrates a decrease in spatial variability, implying that extreme precipitation events tend to be more spatially homogeneous, which may have a severe impact on water resources, agriculture and soil erosion, particularly when associated with desertification risks. Copyright © 2009 Royal Meteorological Society

KEY WORDS precipitation extremes; space–time patterns; stochastic simulation; spatial uncertainty

Received 2 September 2008; Revised 16 July 2009; Accepted 16 July 2009

1. Introduction

Although there is a general agreement on the trend decline of precipitation over the years, the most important factors on desertification and other social and environmental short-term impacts in Mediterranean regions are extreme precipitation events – severe droughts and floods. In Mediterranean climate regions, precipitation patterns are highly variable as far as the time, space, amount and duration of the events is concerned. Most of the studies and projections of future precipitation patterns, based on past observed records and climate change scenarios for the Mediterranean Basin, indicate a decrease in rainfall amounts over the years and an increase in the frequency of heavy/intense rainfall events in autumn and winter seasons, particularly in winter (Brunetti *et al*., 2001; Kostopoulou and Jones, 2005). In some regions, the increasing number of heavy precipitation events increases the flood risk (Hidalgo *et al*., 2003).

Issues such as drought and erosive rainfall have been raising concern about the risks of land degradation and desertification (Lázaro *et al*., 2001). These changes in extreme precipitation events may also have severe implications and impacts on soil erosion, resulting in increased soil degradation risks.

A common tool used to understand and assess the precipitation pattern over a region is the extreme precipitation indices based on daily precipitation series, as indicators of climate change (Jones *et al*., 1999; Karl *et al*., 1999; Brunetti *et al*., 2001). Generally, these indices can be split into two main categories: one involves arbitrary fixed thresholds, such as the number of days per year with daily precipitation exceeding a specific amount or threshold (in millimetres) (e.g. Klein Tank and Können, 2003; Kostopoulou and Jones, 2005) and the other category is based on statistical quantities such as percentiles, which are more appropriate for regions that contain a broad range of climates (Haylock and Nicholls, 2000;

* Correspondence to: R. M. Durão, Instituto Superior Técnico - CERENA, Av. Rovisco Pais, 1049-001 Lisboa, Portugal.
E-mail: rmdurao@ist.utl.pt

Klein Tank and Können, 2003). The use of extreme precipitation indices is recommended by the joint working group on climate change detection of the World Meteorological Organization – Commission for Climatology (WMO-CCL), the Research Programme on Climate Variability and Predictability (CLIVAR) (Peterson *et al*., 2001) and the CLIVAR/GCOS (Global Climate Observing System)/WMO workshop on indices and indicators for climate extremes (Karl *et al*., 1999). From the list of recommended indices, two precipitation indices, one representing wet conditions (R30) and the other representing dry conditions (RL10) have been selected in this work.

The RL10 is defined as the number of days per year with precipitation below 10 mm and the R30 index is based on the count of days per year exceeding a fixed threshold (30 mm). The use of annual indices greatly simplifies the analysis of extremes and provides useful measures for impact analysis as they can be related with extreme events that affect human society and the natural environment (Klein Tank and Können, 2003).

Most of the studies based on extreme precipitation indices only focus on temporal trends rather than space–time patterns and trends (Serrano *et al*., 1999; Klein Tank and Können, 2003; Kostopoulou and Jones, 2005; Moberg and Jones, 2005; Rodrigo and Trigo, 2007; Costa and Soares, 2008).

Rodrigo and Trigo (2007) presented an analysis of precipitation changes across the Iberian Peninsula using a seasonal and annual aggregation of observed precipitation data and showed that main changes occurred in the precipitation intensity of northern and southern stations, with a decreasing trend over time, suggesting that further work will be necessary to obtain a complete view of the spatial–temporal variability of daily precipitation in the Iberian Peninsula.

Costa *et al*. (2008) provide a first insight on the dynamics of three extreme precipitation indices in southern Portugal. Their results do not show any statistically significant linear trends in the regional-average series of the indices (RL10, R30 and R5D: highest consecutive 5-day precipitation total) within the period 1941–2000.

In order to accommodate the spatial dimension to precipitation data analysis, some geostatistical studies have already been carried out, but have been mainly focused on the spatial interpolation of precipitation (e.g. Prudhomme and Reed, 1999; Goovaerts, 2000; Daly, 2006). However, there are very few studies on the modelling of space–time patterns of extreme precipitation indices. Hundecha and Bárdossy's work (2005) interpolated daily precipitation measurements on a 5×5 km grid through external drift kriging, using a digital elevation model as secondary information, and, afterwards, several extreme precipitation indices were calculated on grids of 5, 10, 25 and 50 km.

A different approach is proposed in this work, as the extreme precipitation indices are calculated directly from daily precipitation measurements and then the spatial distribution of extreme precipitation events are analysed using a geostatistical methodology. The semivariograms of extreme precipitation series were modelled and the direct sequential simulation was performed to illustrate the relationships between spatial and temporal extreme precipitation patterns.

A description of the study region and data is presented in Section 2, and the applied methodology is briefly described in Section 3. The obtained results are presented and discussed in Section 4, and the major conclusions are stated in Section 5.

2. Study region and data

2.1. Study region

The study region corresponds to the southern part of continental Portugal, which comprises two different administrative regions, Alentejo and Algarve, having different physiographic characteristics. In the far south, the relief is dominated by the two main Algarve's mountains: Monchique on the west, and Caldeirão on the east. In contrast, the Alentejo region is characterized mainly by vast flat to rolling country, the peneplain, where the average altitude is approximately 200 m. The São Mamede mountain ridge, the highest in the Alentejo region with an altitude of 1000 m, lies in the extreme north-east. These regions are characterized by a Mediterranean climate and present a high level of susceptibility to drought events and desertification phenomena (e.g. Pereira *et al*., 2006).

The precipitation regime in southern Portugal is characterized by highly irregular behaviour in both the spatial and temporal dimensions, namely in the amount and distribution of rainfall (Daveau, 1977). Given the impacts of droughts and floods, the study of extreme precipitation space–time variability is of paramount importance in terms of water basins management in the south of the Iberian Peninsula (Ramos and Reis, 2002; Trigo *et al*., 2004).

The precipitation regime in Portugal can be explained by two different seasonal atmospheric mechanisms. In summer, the large-scale atmospheric circulation is steered by the Azores anticyclone, which is displaced towards its north-westerly position, producing northerly or north-easterly winds that bring warm and dry air into Continental Portugal, which is either of continental or of maritime origin. However, in southern Portugal, summer precipitation is sometimes associated with local convective activity. On the other hand, during winter, the large-scale circulation is mainly driven by the position and intensity of the Icelandic low, and Portugal is affected by westerly winds that carry moist air and produce rainfall events mainly in northern Portugal (Trigo and DaCamara, 2000).

2.2. Data

The monitoring network utilized is an original set of 38 (decade of 1960) to 106 monitoring stations (decade of 1990) with daily precipitation data (Figure 1). The data set was compiled from the National System of Water Resources Information database (SNIRH – Sistema

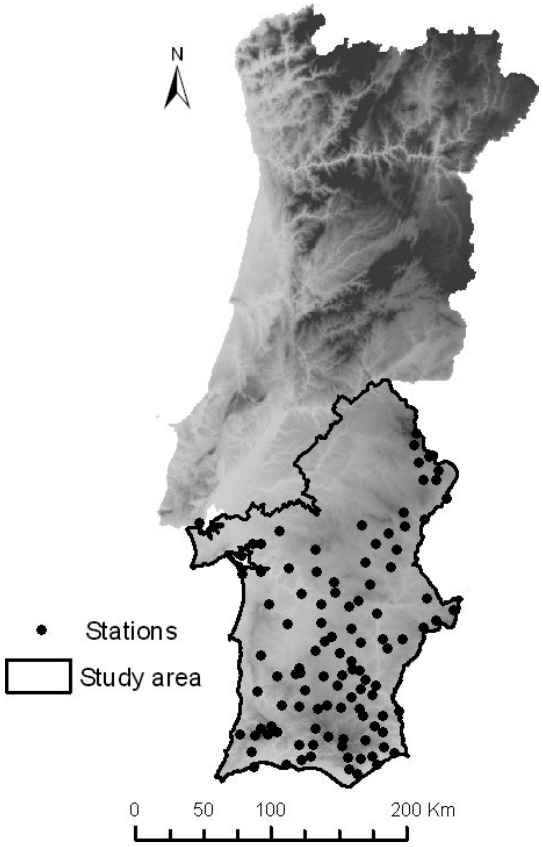

Figure 1. Study domain and stations' locations with selected daily precipitation series.

Nacional de Informação de Recursos Hídricos, http://snirh.inag.pt) and three daily series were compiled from the European Climate Assessment (ECA) dataset (http://eca.knmi.nl). All precipitation time series were quality controlled by several procedures (e.g. Costa and Soares, 2006, 2009).

Extreme precipitation indices are sensitive to the number of missing days, thus using a similar approach as proposed by Haylock and Goodess (2004). Therefore, for each station, the indices for a specific year were set to missing if there were more than 16% of the days missing for that year (Costa and Soares, 2009). The annual extreme precipitation indices (RL10, R30) were computed using the selected daily precipitation series.

The RL10 index is defined as the number of days per year with precipitation below 10 mm. Although the 10-mm threshold cannot be considered very low in terms of precipitation, it fits the extreme events regime of the study area: the average number of days with precipitation below 10 mm is greater than 330.

The index R30 measures the frequency of heavy precipitation events and is defined as the number of days per year with precipitation equal to or more than 30 mm. This threshold fits the extreme events regime of the region under study, as it corresponds approximately to the 99% regional-average percentile of the 1961–1990 climate normal (see Table I).

Table I. Basic statistics of the daily precipitation data (in mm).

Basic statistics	Study period (1961–2000)	Climate-normal (1961–1990)
Mean	1.727	1.764
Median	0	0
Std. deviation	5.995	6.002
Sample variance	35.946	36.028
Kurtosis	71.917	62.299
Skewness	6.642	6.337
Range	274.7	186
Minimum	0	0
Maximum	274.7	186
Percentile 100% (max)	274.7	186
Percentile 99%	29.1	29.3
Percentile 95%	11.2	11.5
Percentile 90%	4.9	5
Percentile 75%	0	0
Percentile 50%	0	0
Percentile 25%	0	0
Percentile 10%	0	0
Percentile 5%	0	0
Percentile 1% (min)	0	0

3. Space–time pattern's assessment

The space–time patterns of extreme precipitation indices over the study region were evaluated using geostatistical methods. In this work, a simple approach to space–time modelling was adopted treating time simply as an additional dimension, and traditional geostatistical techniques were applied to the (2D+1) space–time domain (Eynon and Switzer, 1983; Kyriakidis and Journel, 1999).

The selected geostatistical methodology was applied in two stages:

- in the first one, the extreme precipitation indices were computed for each monitoring station and the space–time semivariograms were obtained for the given period;
- in the second stage, stochastic simulation (direct sequential simulation algorithm) was used to evaluate the mean spatial pattern and the local variability of the extreme precipitation indices.

The semivariogram is a correlation function of distance between two points, which summarizes the main spatial continuity patterns of the selected precipitation indices.

The direct sequential simulation approach belongs to a family of stochastic sequential simulation techniques, which aims at generating images of a given spatial random function with the same spatial characteristics (semivariograms, histograms) as the experimental data (Goovaerts, 1997; Soares, 2001). DSS is used to illustrate (and emphasize) the main conclusions about the space–time patterns of extreme precipitation indices.

3.1. Semivariograms

The semivariogram is the geostatistical key function and it characterizes the variability of the spatial (and temporal) patterns of a certain phenomena. The experimental semivariogram or sample variogram $\hat{\gamma}(h)$ is computed as half the average squared difference between data pairs belonging to a certain distance class:

$$\hat{\gamma}(h) = \frac{1}{2N(h)} \sum_{\alpha=1}^{N(h)} [z(u_\alpha) - z(u_\alpha + h)]^2 \qquad (1)$$

where $N(h)$ is the number of pairs for a distance class.

The semivariogram models and their parameters are estimated taking into account the experimental semivariograms that are computed from data values. The main objective is to capture the spatial pattern of the physical phenomenon in the variogram model rather than getting a best fit of a second moment (Goovaerts, 1997).

Typically, a mathematical semivariogram model is selected from a small set of admissible functions (e.g. exponential or spherical) and is fitted to experimental semivariogram values calculated from data for certain angular and distance classes.

The parameters of the semivariogram model (sill, range and nugget) are used to assign optimal weights for spatial prediction using kriging or stochastic simulation.

In bounded models (e.g. spherical and exponential), semivariogram functions increase with distance until they reach a maximum, named *sill*, at an approximate distance known as the *range*. The range is the distance h at which the spatial (or temporal) correlation vanishes, i.e. observations separated by a distance larger than the range are spatially (or temporally) independent observations. The range is one of the most important parameters because it is related with the spatial (or space–time) extent of continuity of the phenomenon. The nugget effect (C_0) is determined when h approaches 0 and results from high variability at short distances that can be caused by lack of samples, or sampling inaccuracy.

The semivariogram is usually modelled by a visual fitting procedure using a graphical interface. Least squares techniques can provide an automatic fit of the experimental variogram. In the course of a detailed geostatistical analysis, an automatic fit rarely provides definitive results. At most it can be the first step of a visual fit (Chilés and Delfiner, 1999). The automatic procedures are roughly classified into two categories: full black-box and semi-automatic. The first is generally disapproved by geostatisticians because it is an uncontrolled process and the results are often senseless (Goovaerts, 1997; Webster and Oliver, 2007). The semi-automatic procedures rely critically on a series of user's decisions, which must be backed by experimental data or ancillary information (Goovaerts, 1997). Actually, at the end the semi-automatic procedure adds little to the fitting process, because the recommended procedure suggests that the final decision should be based on a visual inspection of the result.

3.2. Direct sequential simulation

Geostatistical simulation has been used to characterize the space–time uncertainty of physical phenomena in Earth and environmental sciences applications (Kyriakidis and Journel, 1999; Soares and Pereira, 2007; Russo *et al*., 2008), which is the main objective of this work.

The aim of sequential simulation is to generate a set of equiprobable realizations of a random field, rather than the most probable realization (given, for example, by least squares interpolators). Each simulated image reproduces the main spatial patterns as revealed by semivariograms inferred by the experimental data (Journel, 1994; Goovaerts, 1997; Soares, 2001).

Let us consider $Z(u)$, a continuous random function Z, for any spatial and temporal location u. $Z(u)$ has a global cumulative distribution function (cdf):

$$F_z(z) = \text{prob}\,\{Z(u) < z\} \qquad (2)$$

and a stationary semivariogram $\gamma(h)$.

The objective is to simulate realizations of random function $Z(u)$, which reproduce both $F_z(z)$ and $\gamma(h)$.

Soares (2001) describes the sequence of the direct sequential simulation (DSS) algorithm of a continuous variable as follows:

1. Define a random path over an entire grid of nodes u_i, $i = 1, N$, to be simulated. N is the total number of grid nodes to be simulated.
2. Estimate the local mean and variance of $z(u_i)$, identified, respectively, by the simple kriging estimate $z(u_i)^*$ and estimation variance, $\sigma^2_{sk}(u_i)$, conditioned to the experimental data $z(u_\alpha)$ and previous simulated values $z^{\mathrm{l}}(u_i)$.
3. Draw a value $z^{\mathrm{l}}(u_i)$ by sampling from the global histogram a value centred in the estimated local mean and variance.
4. Return to step (1) until all N nodes have been visited by the random path.

The set of simulated spatial images $Z^{\mathrm{l}}(u)$, $\mathrm{l} = 1$ to N_s realizations can give rise to the most probable image (E-type map):

$$Z(u_i)^* = \frac{\sum_{l=1}^{N_s} Z^l(u_i)}{N_s} \qquad (3)$$

The spatial uncertainty can also be derived from simulated images by calculating the variance for each simulation node:

$$\text{Var}(u_i) = \sum_{l=1}^{N_s} \left(Z^l(u_i) - Z(u_i)^*\right)^2 \qquad (4)$$

Table II. Basic Statistics of the RL10 index per decade (number of days per year with precipitation <= 10 mm).

Decade	Min.	Median	Mean	Var.	Std. dev.	Max.	Samples
1961–1970	305	341	339	81.38	9.02	359	339
1965–1974	309	345	343.99	66.78	8.17	360	353
1971–1980	309	345	343.93	60.97	7.81	360	365
1975–1984	312	347.5	346.46	56.08	7.49	363	488
1981–1990	306	347	344.29	94.45	9.72	363	755
1985–1994	306	348	344.93	83.5	9.14	361	910
1991–1900	305	347	345.73	70.66	8.41	363	864

Table III. Basic statistics of the R30 index per decade (number of days per year with daily rainfall above or equal to 30 mm).

Decade	Min.	Median	Mean	Var.	Std. dev.	Max.	Samples
1961–1970	0	3	4.08	9.98	3.16	20	339
1965–1974	0	2	3.16	8.62	2.94	15	353
1971–1980	0	2	3.21	9.51	3.08	16	365
1975–1984	0	2	2.94	7.68	2.77	16	488
1981–1990	0	2	3.53	13.09	3.62	23	755
1985–1994	0	2	3.28	11.86	3.44	23	910
1991–2000	0	3	3.24	8.98	3.0	18	864

The above algorithm can be used to simulate any continuous random variable. In this case study, both equations Equations (3) and (4) were used to obtain the most probable image of the RL10 and R30 per decade, and a measure of the spatial uncertainty, respectively.

4. Results and discussion

4.1. Space–time continuity analysis

The RL10 and R30 extreme precipitation indices were computed for each monitoring station using data within the period 1961–2000. Having in mind the purpose of detecting spatial–temporal changes in the indices behaviour, the data were grouped in seven 10-year periods: 1961–1970, 1965–1974, 1971–1980, 1975–1984, 1981–1990, 1985–1994 and 1991–2000.

Basic statistics of RL10 and R30 indices per decade are presented in Tables II and III in order to characterize their behaviour over the period of study. Both indices present similar statistics over decades, despite the fact that the number of samples in space has tripled during the study period. The RL10 presents a minimum of about 305 and maximum of 363 with a mean between 339 and 346 and a variance ranging from 56 to 94.

The R30 exihibits a minimum of 0 and a maximum of 23 with a variance of around 10.

Space–time semivariograms (covariances) were then calculated to assess the spatial–temporal correlation between monitoring stations during each 10-year period. After the calculation of experimental semivariograms, a theoretical model was fitted to the experimental semivariogram. Visual (manual) fitting was applied giving more importance to its behaviour near the origin (the smaller lags), which is statistically more consistent (more pair of points) and more important for any spatial prediction. At the end, one must have a fitted model that honours the experimental semivariogram values and reveals the major spatial and temporal features of the attribute under study within each decadal period.

Taking into account the previous considerations, the semivariogram model that best fitted the experimental variograms was the spherical model, which is a function of two parameters:

$$\gamma(h) = \begin{cases} C & \left[1.5\frac{h}{a} - 0.5\left(\frac{h}{a}\right)^3\right] \; if \quad h \le a \\ C & \text{otherwise} \end{cases} \tag{5}$$

where a is the range and C is the sill. The model reaches the sill at a distance a.

In the case of the models fitted to R30 decadal experimental semivariograms, a nugget effect, C_0, was added to the spherical structure.

Considering the results of a thorough analysis on directional semivariograms, isotropic semivariogram models were fitted. The results are presented in Figures 2–5, and the semivariogram parameters are summarized in Tables IV and V.

The range of the spatial component of RL10 semivariograms (Figure 2 and Table IV) has been increasing continuously over decades, from the 40 km range in the 1965–1974 to 65 km in the 1991–2000. Moreover, the corresponding sill parameter does not vary substantially over decades and never reaches the experimental variance (*a priori* variance). In what concerns to the time dimension of this index (Figure 3 and Table IV), the range varied between 1 and 6 years, but no trends were

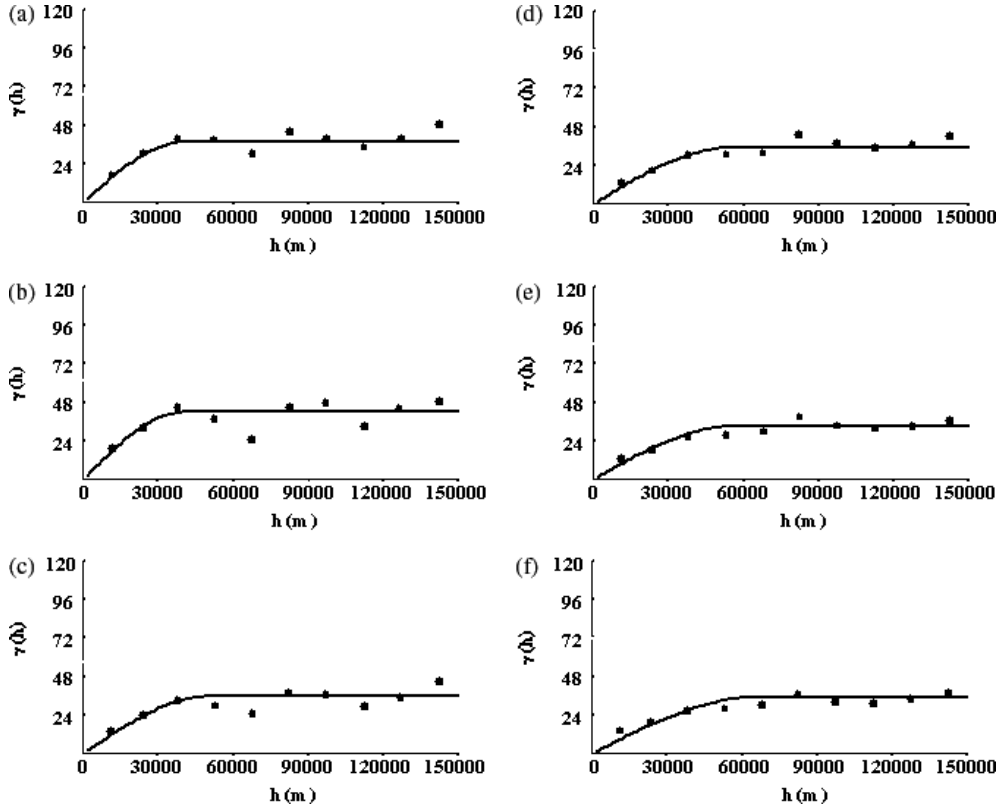

Figure 2. Spatial component of RL10 index experimental semivariograms and spherical models fitted. Graphs show the spatial component for the decades: (a) 1965–1974, (b) 1971–1980, (c) 1975–1984, (d) 1981–1990, (e) 1985–1994 and (f) 1991–2000, respectively.

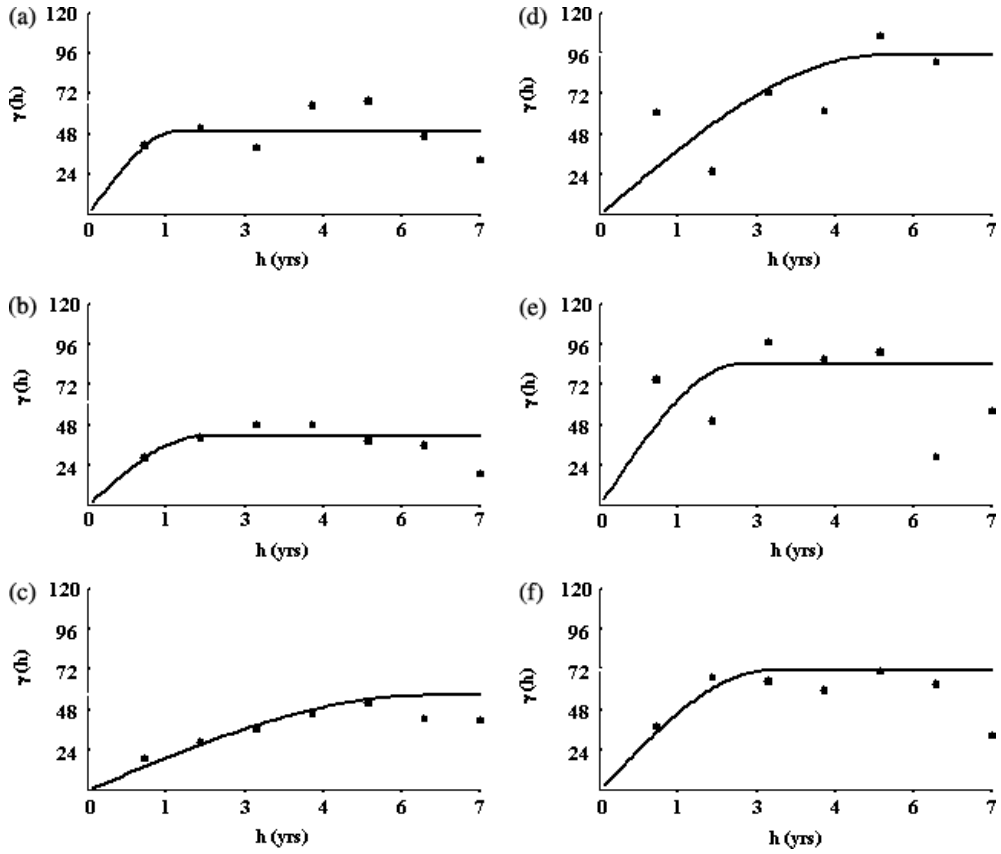

Figure 3. Temporal component of RL10 index experimental semivariograms and spherical models fitted. Graphs show the temporal component for the decades: (a) 1965–1974, (b) 1971–1980, (c) 1975–1984, (d) 1981–1990, (e) 1985–1994 and (f) 1991–2000, respectively.

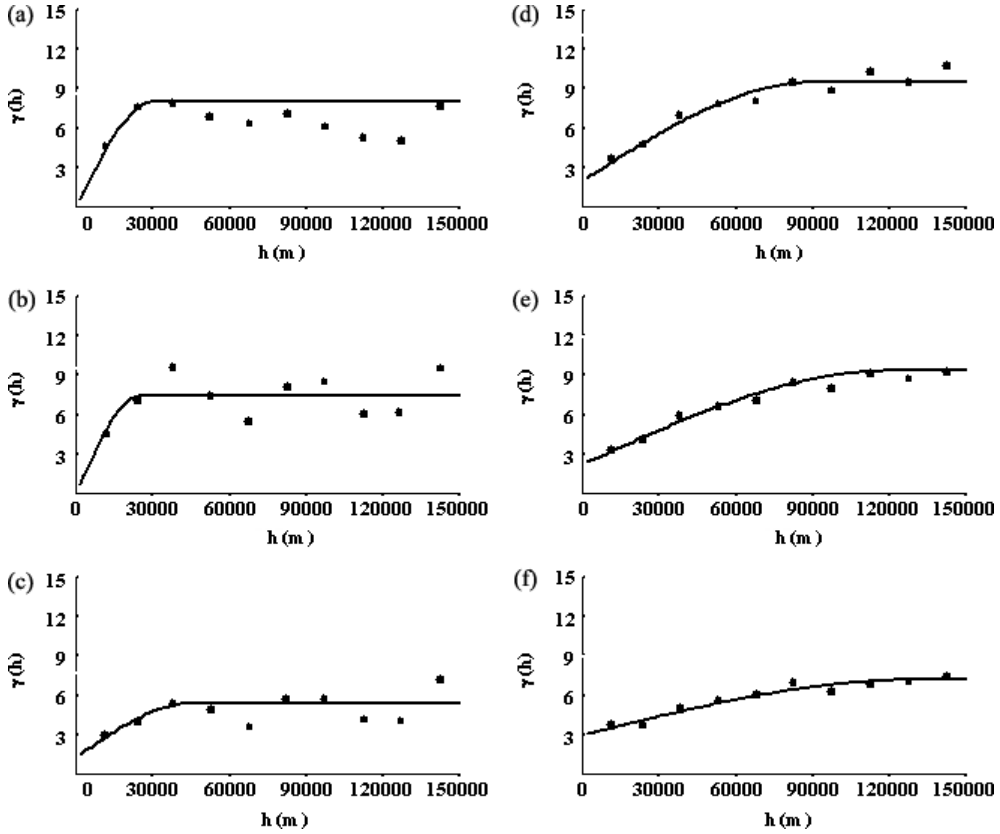

Figure 4. Spatial component of R30 index experimental semivariograms and spherical models fitted. Graphs show the spatial component for the decades: (a) 1965–1974, (b) 1971–1980, (c) 1975–1984, (d) 1981–1990, (e) 1985–1994 and (f) 1991–2000, respectively.

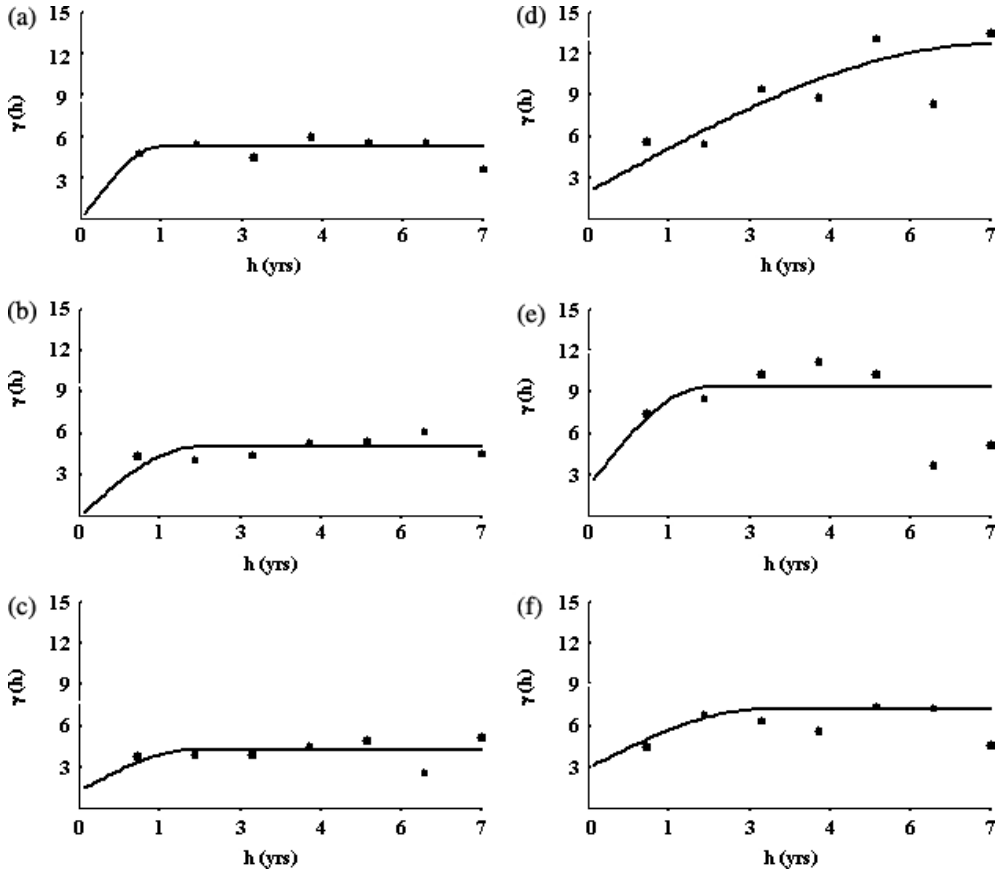

Figure 5. Temporal component of R30 index experimental semivariograms and spherical models fitted. Graphs show the temporal component for the decades: (a) 1965–1974, (b) 1971–1980, (c) 1975–1984, (d) 1981–1990, (e) 1985–1994 and (f) 1991–2000, respectively.

Table IV. Parameters of the space–time semivariograms for the RL10 index per decade.

Decade	Spatial Range a1 (m)	Temporal Range a1 (years)	Sill (Spatial) C1	Sill (Temp.) C1
1965–1974	40 000	1.6	39	50
1971–1980	40 000	2	42	41
1975–1984	50 000	6	36	56
1981–1990	55 000	5	35	95
1985–1994	55 000	2.5	33	84
1991–2000	65 000	3	35	71

Table V. Parameters of the space–time semivariograms for the R30 index per decade.

Decades	Spatial(range) a1 (m)	Temp(range) a1 (years)	Nugget(spat) C0	Nugget(temp) C0	Sill(spat) C1	Sill(temp) C1
1965–1974	30 000	1.4	0	0	8	5.3
1971–1980	25 000	2	0	0	7.5	5
1975–1984	45 000	2	1.3	1.3	4.1	3
1981–1990	90 000	7	2	2	7.5	7.2
1985–1994	120 000	2	2.25	2.25	7.1	7.1
1991–2000	130 000	3	3	3	4.2	4.2

detected, i.e. ranges were neither increasing nor decreasing over decades. In most of the cases, the sill did not reach the experimental variance, which is a very common situation characterized by 'zonal anisotropy' (Goovaerts, 1997); it means that, in a given direction, the phenomenon is extremely homogeneous and the variability is lower than the *a priori* variance (global variability measure) computed from data. The results shown by the R30 are similar to those in the previous index, RL10, but the increase in the spatial continuity is more significant; the ranges of the spatial component of the R30 shows a substantial increase over decades, from the 30 km range in 1965–1974 to 130 km in 1991–2000 (Figures 4–5 and Table V). Additionally, R30 semivariograms also exhibit an increase in the 'nugget effect' over decades, which mean an increase in spatial variability at very small distances, while an increase in the homogeneity at the large distances scale. Further investigation is needed to understand what physical processes explain this result: the phenomenon is increasingly continuous in space but, at the same time, presents more erratic fluctuations at small distances (different values of monitoring stations close to each other). On the other hand, the time component of R30 semivariogram parameters still does not present any trend.

Figure 6 shows the increase in the semivariograms spatial ranges over time for both indices, by means of simple linear regressions based on the least square procedure. The determination coefficients for this linear regression were 0.96 and 0.94 for RL10 and R30 respectively. This figure emphasizes what was already noted by the analysis of Table IV and V, implying that extreme events tend to be more spatially homogeneous through time in this region especially in what concerns to the R30 index.

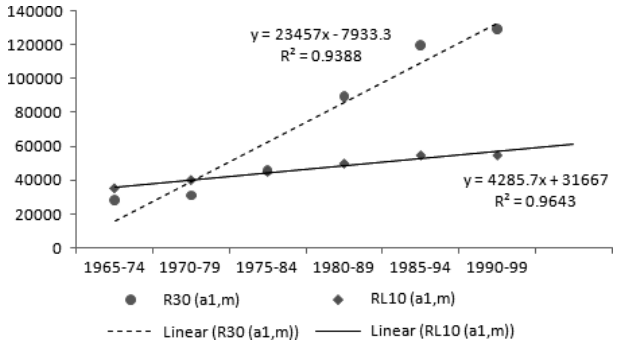

Figure 6. RL10 and R30 indices obtained trends.

4.2. Space–time patterns of extreme precipitation indices

The space patterns over decades of the indices can be visualized with maps generated by direct sequential simulation on 800×800 m grid cells, using the semivariogram models previously fitted for each 10-year period.

Spatial patterns, as revealed by the semivariograms, are reproduced in the simulation of spatial random fields by performing direct sequential simulations. The simulation algorithm generates a set of realizations of the spatial phenomenon with the same probability distribution function: semivariograms of RL10 and R30 indices calculated from precipitation data series. For each 10-year period, 100 equiprobable simulated images were computed and the local uncertainty was assessed through variance maps of the set of equiprobable simulated images, computed at each grid node.

E-type maps, i.e. the average of simulated maps (Goovaerts, 1997; Deutsch and Journel, 1998), give a mean image of R30 and RL10 indices per decade,

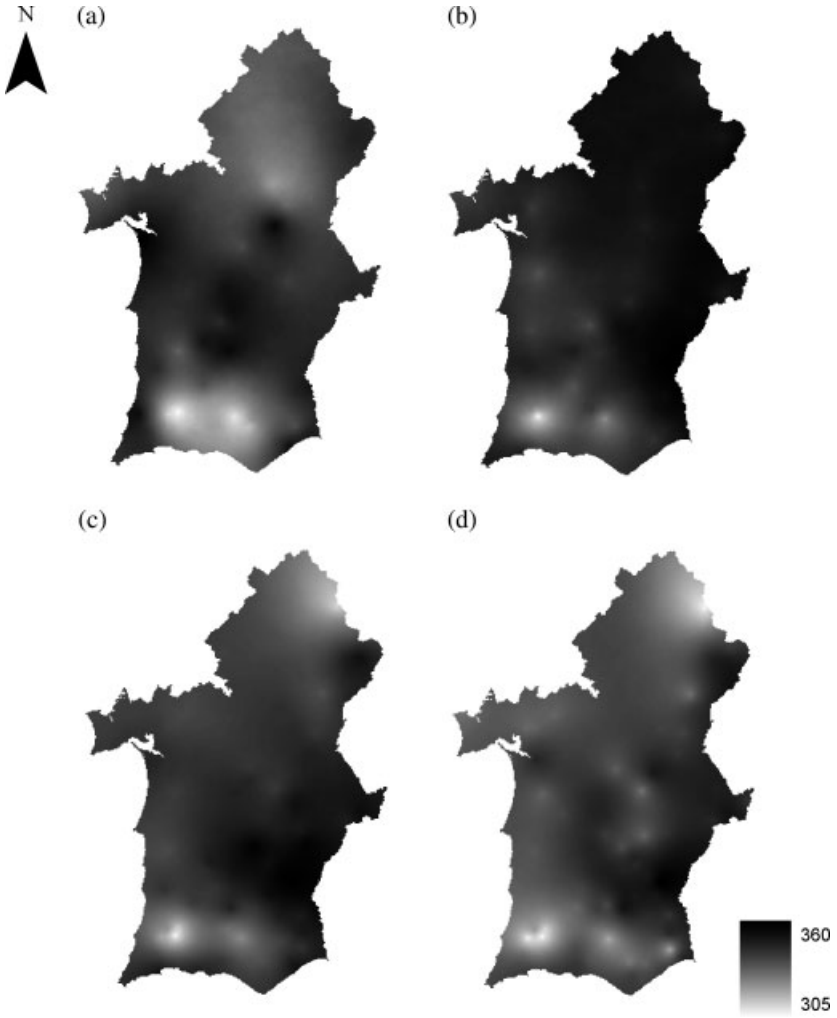

Figure 7. E-type maps of the RL10's driest year per decade (1964, 1974, 1982 and 1992).

while the local variability maps enable the quantification of spatial variability/homogeneity of each index per decade. E-type maps of RL10's driest year per decade (1964, 1974, 1982 and 1992) are presented in Figure 7, and analogous maps of R30's wettest year per decade (1969, 1979, 1989 and 1996) are presented in Figure 8. The associated local variances of the equiprobable images are presented in Figures 9 and 10, respectively. The obtained results o illustrate the conclusions drawn from the variogram analysis, i.e. the levels of local variability are decreasing over time, implying that these indices are more homogenous over time.

Hence, two main conclusions can be drawn:

1. Spatial variability, as can be seen from the semivariogram ranges, has decreased over time since the 1961–1970 up to 1991–2000, which means that extreme phenomena (RL10 and R30 indices) have become more spatially homogeneous since then.
2. This reduction in overall spatial variability can also be seen from the local variability maps, in which local variances tend to decrease over time, especially in the R30 index.

This analysis also shows that despite no evidence of any time trend of the average behaviour of these indices, there is a clear trend of the spatial variability/homogeneity over the decades. In other words, the spatial distributions of the two precipitation indices show an increase in the spatial continuity over time, as expected from the analysis of the experimental space–time semivariograms in the previous section and according to the observed decrease in the local variability.

5. Conclusions

The main objective of this paper is to assess the spatial–temporal dynamics of extreme precipitation in southern Portugal. The space–time patterns of two extreme precipitation indices were estimated from a set of 105 monitoring stations with records within the period 1961–2000. Space–time semivariograms were computed for several 10-year periods, which allowed the characterization of the indices' space–time continuity patterns.

From the 1965–1974 decade until the end of the last century, a clear trend of the spatial extent of extreme

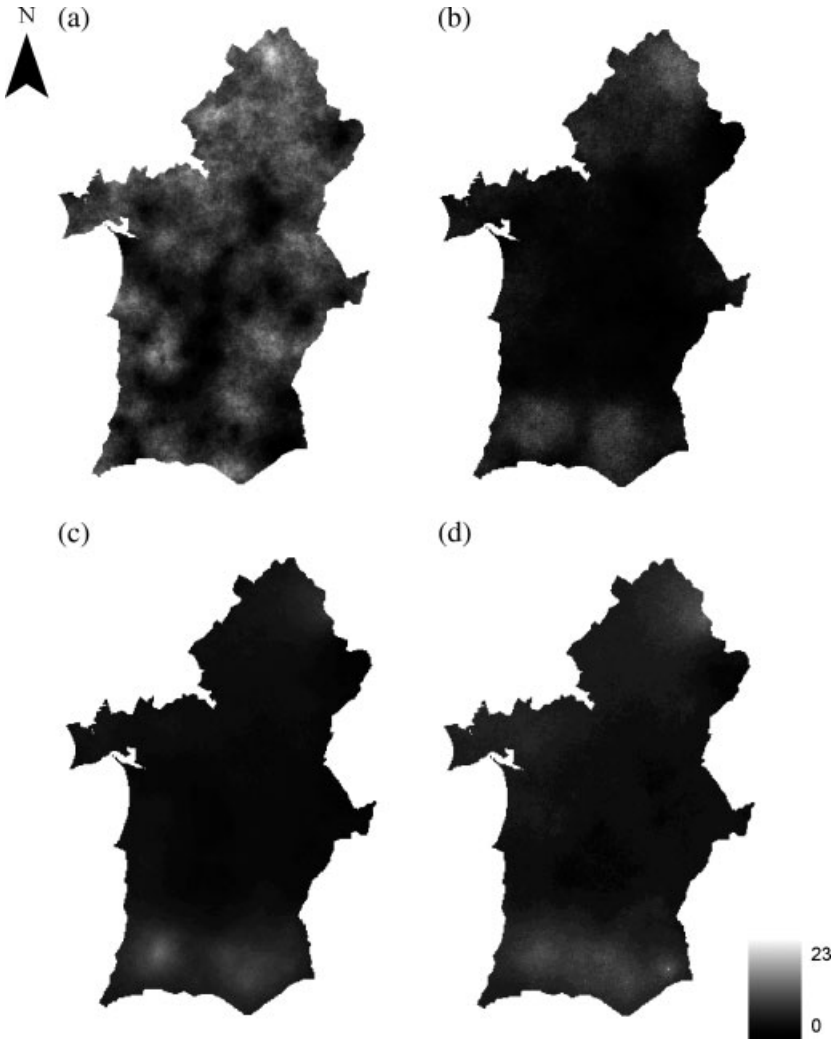

Figure 8. E-type maps of R30's wettest year per decade (1969, 1979, 1989 and 1996).

phenomena has been observed and measured. Although the yearly mean and global variances of the indices do not change significantly in that period, the spatial correlation between monitoring stations increases significantly over that period. This means that extreme events tend to be more spatially homogeneous, i.e. to have a larger spatial continuity over time.

Therefore, the following main conclusion can be drawn: both extreme precipitation indices, RL10 (frequency of dry precipitation events) and R30 (frequency of extremely heavy precipitation events), show increasing spatial continuity through time, implying that the spatial patterns are more homogenous in recent times. This is an extremely important input for the short- and medium-term management of Portuguese water basins.

This new approach that accounts for spatial patterns for characterizing and evaluating climate change could be applied to other regions under environmental stress, such as drought and desertification. The recognition of changes in precipitation indices, more evident in space than in time, will bring further understanding of climate change effects and impacts, and is likely to have substantial implications in the planning and management of natural resources, especially of regions with high desertification risk where these are critical issues. Therefore, the links between large-scale atmospheric mechanisms and the observed trends in the spatial homogeneity of these extremes precipitation indices will be the subject of a future work in order to obtain a complete study of their space–time variability.

Acknowledgements

This paper was developed in the framework of the following projects: BioAridRisk – Space-Time Evaluation of the Risks of Climate Change Based on an Aridity Index (POCI/CLI/56371/2004FCT/MCTES), CIDmeg – Construction of a Desertification Susceptibility Index for the Left Margin of Guadiana (POCI/CLI/58865/2004 FCT/MCTES) and SADMO – Système d'Évaluation et Contrôle de la Désertification dans la Méditerranée Occidentale (Programme Interreg IIIB, MEDDOC, CONVENTION n. 2005-05-4.4-P-105).

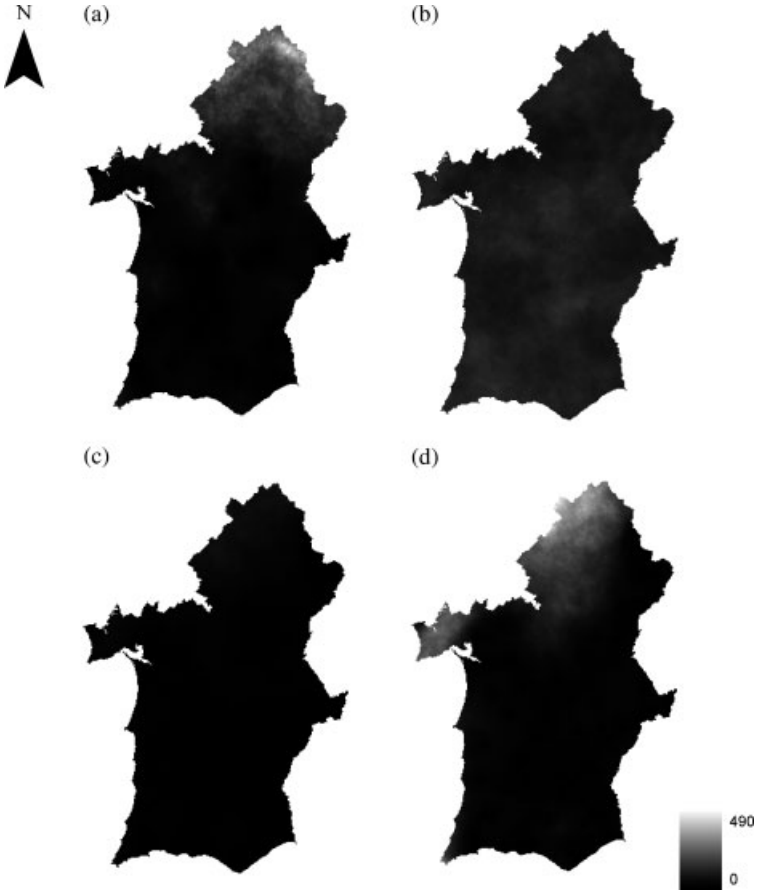

Figure 9. Local variability of RL10's driest year: (a) 1964, (b) 1974, (c) 1982 and (d) 1992.

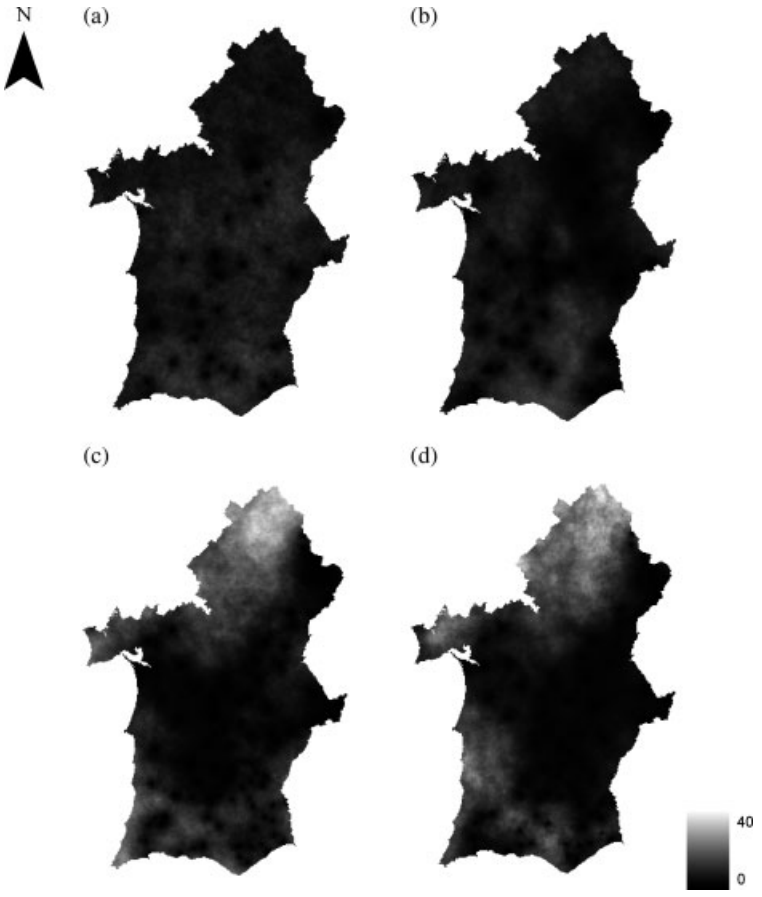

Figure 10. Local variability of R30's wettest year: (a) 1969, (b) 1979, (c) 1989 and (d) 1996.

References

Brunetti M, Colacino M, Maugeri M, Nanni T. 2001. Trends in the daily intensity of precipitation in Italy from 1951 to 1996. *International Journal of Climatology* **21**(3): 299–316.

Chiles JP, Delfiner P. 1999. *Geostatistics: Modeling Spatial Uncertainty*. John Wiley and Sons: New York.

Costa AC, Durão R, Pereira MJ, Soares A. 2008. Using stochastic space-time models to map extreme precipitation in southern Portugal. *Natural Hazards and Earth System Sciences* **8**(4): 763–773.

Costa AC, Soares A. 2006. Identification of inhomogeneities in precipitation time series using SUR models and the Ellipse test. In *Proceedings of Accuracy 2006–7th International Symposium on Spatial Accuracy Assessment in Natural Resources and Environmental Sciences*, Caetano M, Painho M (eds). Instituto Geográfico Português: Portugal; 419–428.

Costa AC, Soares A. 2008. Trends in extreme precipitation indices derived from a daily rainfall database for the South of Portugal. *International Journal of Climatology.* DOI: 10.1002/joc.1834.

Costa AC, Soares A. 2009. Homogenization of climate data: review and new perspectives using geostatistics. *Mathematical Geosciences* **41**(3): 291–305.

Daly C. 2006. Guidelines for assessing the suitability of spatial climate data sets. *International Journal of Climatology* **26**(6): 707–721.

Daveau S. 1977. Répartition et rythme des précipitations au Portugal. Memórias C.E.G, 3, Lisbon.

Deutsch C, Journel A. 1998. *GSLIB: Geostatistical Software Library and User's Guide*, 2nd edn. Oxford University Press: New York.

Eynon BP, Switzer P. 1983. The variability of rainfall acidity. *Canadian Journal of Statistics* **11**: 11–24.

Goovaerts P. 1997. *Geostatistics for Natural Resources Evaluation*. Oxford University Press: New York.

Goovaerts P. 2000. Geostatistical approaches for incorporating elevation into the spatial interpolation of rainfall. *Journal of Hydrology* **228**: 113–129.

Haylock MR, Goodess CM. 2004. Interannual variability of European extreme winter rainfall and links with mean large-scale circulation. *International Journal of Climatology* **24**(6): 759–776.

Haylock M, Nicholls N. 2000. Trends in extreme rainfall indices for an updated high quality data set for Australia, 1910–1998. *International Journal of Climatology* **20**(13): 1533–1541.

Hidalgo JCG, De Luís M, Raventós J, Sánchez JR. 2003. Daily rainfall trend in the Valencia Region of Spain. *Theoretical and Applied Climatology* **75**: 117–130.

Hundecha Y, Bárdossy A. 2005. Trends in daily precipitation and temperature extremes across western Germany in the second half of the 20th century. *International Journal of Climatology* **25**(9): 1189–1202.

Jones PD, Horton EB, Folland CK, Hulme M, Parker DE, Basnett TA. 1999. The use of indices to identify changes in climatic extremes. *Climatic Change* **42**: 131–149.

Journel AG. 1994. Modeling uncertainty: some conceptual thoughts. In *Geostatistics for the Next Century*, Dimitrakopoulos R (ed.). Kluwer Academic Publishers: Dordrecht; 30–43.

Karl TR, Nicholls N, Ghazi A. 1999. CLIVAR/GCOS/WMO Workshop on indices and indicators for climate extremes. Workshop summary. *Climatic Change* **42**: 3–7.

Klein Tank AMG, Können GP. 2003. Trends in indices of daily temperature and precipitation extremes in Europe, 1946–1999. *Journal of Climate* **16**(22): 3665–3680.

Kostopoulou E, Jones PD. 2005. Assessment of climate extremes in the Eastern Mediterranean. *Meteorology and Atmospheric Physics* **89**: 69–85.

Kyriakidis PC, Journel AG. 1999. Geostatistical space-time models. *Mathematical Geology* **31**(6): 651–684.

Lázaro R, Rodrigo FS, Gutiérrez L, Domingo F, Puigdefábregas J. 2001. Analysis of a 30-year rainfall record (1967–1997) in semi–arid SE Spain for implications on vegetation. *Journal of Arid Environments* **48**(3): 373–395.

Moberg A, Jones PD. 2005. Trends in indices for extremes in daily temperature and precipitation in central and western Europe, 1901–1999. *International Journal of Climatology* **25**: 1149–1171.

Pereira LS, Louro V, Rosário L, Almeida A. 2006. Desertification, territory and people, a holistic approach in the Portuguese context. In *Desertification in the Mediterranean Region: A Security Issue*, Kepner WG, Rubio JL, Mouat DA, Pedrazzini F (eds). NATO Sc.Com., AK/Nato Publishing Unit. Springer-Verlag: Dordrecht; 269–289.

Peterson TC, Folland C, Gruza G, Hogg W, Mokssit A, Plummer N. 2001. Report on the activities of the working group on climate change detection and related rapporteurs 1998–2001. World Meteorological Organisation Rep. WCDMP-47, WMO-TD 1071. Geneva.

Prudhomme C, Reed DW. 1999. Mapping extreme rainfall in a mountainous region using geostatistical techniques: a case study in Scotland. *International Journal of Climatology* **19**(12): 1337–1356.

Ramos C, Reis E. 2002. Floods in southern Portugal: their physical and human causes, impacts and human response. *Mitigation and Adaptation Strategies for Global Change* **7**(3): 267–284.

Rodrigo FS, Trigo RM. 2007. Trends in daily rainfall in the Iberian Peninsula from 1951 to 2002. *International Journal of Climatology* **27**: 513–529. DOI: 10.1002/joc.1409.

Russo A, Trigo R, Soares A. 2008. Stochastic modelling applied to air quality space-time characterization. In *geoENV VI – Geostatistics for Environmental Applications*, Soares A, Pereira MJ, Dimitrakopoulos R (eds). Springer: Netherlands; 83–93.

Serrano A, Mateos VL, García JA. 1999. Trend analysis of monthly precipitation over the Iberian Peninsula for the period 1921–1995. *Physics and Chemistry of the Earth* **24**: 85–90.

Soares A. 2001. Direct sequential simulation and cosimulation. *Mathematical Geology* **33**(8): 911–926.

Soares A, Pereira MJ. 2007. Space–time modelling of air quality for environmental-risk maps: a case study in South Portugal. *Computers & Geosciences* **33**(10): 1327–1336.

Trigo RM, DaCamara C. 2000. Circulation Weather Types and their impact on the precipitation regime in Portugal. *International Journal of Climatology* **20**(13): 1559–1581.

Trigo RM, Pozo-Vázquez D, Osborn TJ, Castro-Díez Y, Gámiz-Fortis S, Esteban-Parra MJ. 2004. North Atlantic oscillation influence on precipitation, river flow and water resources in the Iberian Peninsula. *International Journal of Climatology* **24**(8): 925–944.

Webster R, Oliver MA. 2007. *Geostatistics for Environmental Scientists*, 2nd edn. John Wiley and Sons: New York.

